





Star-forming Rings in Lenticular Galaxies: Origin of the Gas*

Irina S. Proshina¹, Alexei Yu. Kniazev^{1,2,3} , and Olga K. Sil'chenko^{1,4} ¹ Sternberg Astronomical Institute, M.V. Lomonosov Moscow State University, Universitetsky pr., 13, Moscow, 119991, Russia; olga@sai.msu.su, olgasil.astro@gmail.com, ii.pro@mail.ru, akniazev@sao.ac.za² South African Astronomical Observatory, P.O. Box 9, 7935 Observatory, Cape Town, South Africa³ Southern African Large Telescope Foundation, P.O. Box 9, 7935 Observatory, Cape Town, South Africa⁴ Physics Department, M.V. Lomonosov Moscow State University, Russia

Received 2018 November 27; revised 2019 April 24; accepted 2019 April 25; published 2019 June 7

Abstract

Rings in S0s are enigmatic features that can, however, betray the evolutionary paths of particular galaxies. We have undertaken long-slit spectroscopy of five lenticular galaxies with UV-bright outer rings. The observations have been made with the Southern African Large Telescope to reveal the kinematics, chemistry, and ages of the stellar populations and the gas characteristics in the rings and surrounding disks. Four of the five rings are also bright in the H α emission line, and the spectra of the gaseous rings extracted around the maxima of the H α equivalent width reveal excitation by young stars betraying current star formation in the rings. The integrated level of this star formation is 0.1–0.2 $M_{\odot} \text{ yr}^{-1}$, with the outstanding value of 1 $M_{\odot} \text{ yr}^{-1}$ in NGC 7808. The difference of chemical composition between the ionized gas of the rings, which demonstrate nearly solar metallicity, and the underlying stellar disks, which are metal-poor, implies recent accretion of the gas and star formation ignition; the star formation history estimated by using different star formation indicators implies that the star formation rate decreases with an e -folding time of less than 1 Gyr. In NGC 809, where the UV ring is well visible but the H α emission line excited by massive stars is absent, the star formation has already ceased.

Key words: galaxies: abundances – galaxies: elliptical and lenticular, cD – galaxies: evolution – galaxies: ISM – galaxies: star formation – galaxies: structure

1. Introduction

Lenticular galaxies are disk galaxies that differ from spirals by the smooth appearance of their reddish large-scale stellar disks and visible absence of star-forming sites organized as spiral arms. As a class, they belong to the red sequence and are usually characterized as “quiescent” galaxies. However, despite the absence of visible star formation, the disks of S0s often possess noticeable amounts of cold gas (Welch & Sage 2003; Sage & Welch 2006), and to understand what conditions for star formation are lacking in the massive gaseous disks of S0 galaxies is a separate problem (Pogge & Eskridge 1993). The frequent decoupling between the gaseous and stellar kinematics in the S0 disks provoked a suggestion that the cold gas in S0s was mostly accreted from outside (Bertola et al. 1992; Kuijken et al. 1996; Davis et al. 2011; Katkov et al. 2014), and perhaps the conditions of such accretion—off-plane direction of infall and/or intermittent regime of inflow—were often unfavorable for star formation ignition (Katkov et al. 2015). However, when the UV space telescope *GALEX* had surveyed a large sample of nearby galaxies with a spatial resolution of a few arcseconds, numerous UV rings were found in optically red, “quiescent” lenticular galaxies (Gil de Paz et al. 2007; Marino et al. 2011). After the old claims by Pogge & Eskridge (1993) that current star formation in S0s, if present, is concentrated in rings, this feature has been confirmed with the new observational data (Salim et al. 2012).

Outer stellar rings are often present in S0 galaxies. According to the statistics of the recent catalog of stellar rings, ARRAKIS (Comerón et al. 2014), based on the data of the NIR survey of nearby galaxies, S4G (Sheth et al. 2010), the

occurrence of outer stellar rings is maximal just among lenticular galaxies: up to 50% of S0 galaxies ($T = -1$) have outer stellar rings (Comerón et al. 2014). Interestingly, while the fraction of outer rings rises toward the morphological type of -1 , the fraction of strong bars falls (Buta et al. 2010; Laurikainen et al. 2013). This fact puts into doubt the theory that all rings have the resonance nature and are produced by bars (Schommer & Sullivan 1976; Athanassoula et al. 1982; Buta & Combes 1996), at least as concerning the rings in lenticular galaxies. Though the rings found by Comerón et al. (2014) in the data of the *Spitzer* IR space telescope certainly consist of old stars, the subsequent mining in the *GALEX* data has shown that among the outer NIR rings of lenticular galaxies, more than half are also seen in the UV (Kostiuk & Sil'chenko 2015). It means that they contain stars younger than 200 Myr (Kennicutt & Evans 2012), and that recent star formation is common in the outer rings of lenticular galaxies. The next step in the study of the outer rings in S0 galaxies is to look for gas in these rings, see if it is excited by young stars, and deduce something about the origin of the rings based on the gas properties. It is the topic of the present paper.

Here we spectrally study a small sample of five lenticular galaxies where the UV-bright rings are present. In NGC 809 and NGC 7808, the presence of UV rings was reported by Gil de Paz et al. (2007) and measured by Ilyina & Sil'chenko (2011); for NGC 4324, a nice picture of its UV ring is presented by Cortese & Hughes (2009). The distant S0 galaxy PGC 48114 was noted as a ring galaxy by Kostyuk (1975), and our inspection of the corresponding *GALEX* image has confirmed the presence of an extended UV signal in this object. Finally, NGC 2697 has been found by us serendipitously and is confirmed to have a ring morphology in the *GALEX* maps by visual inspection. The literature data on the

* Based on observations made with the Southern African Large Telescope (SALT).

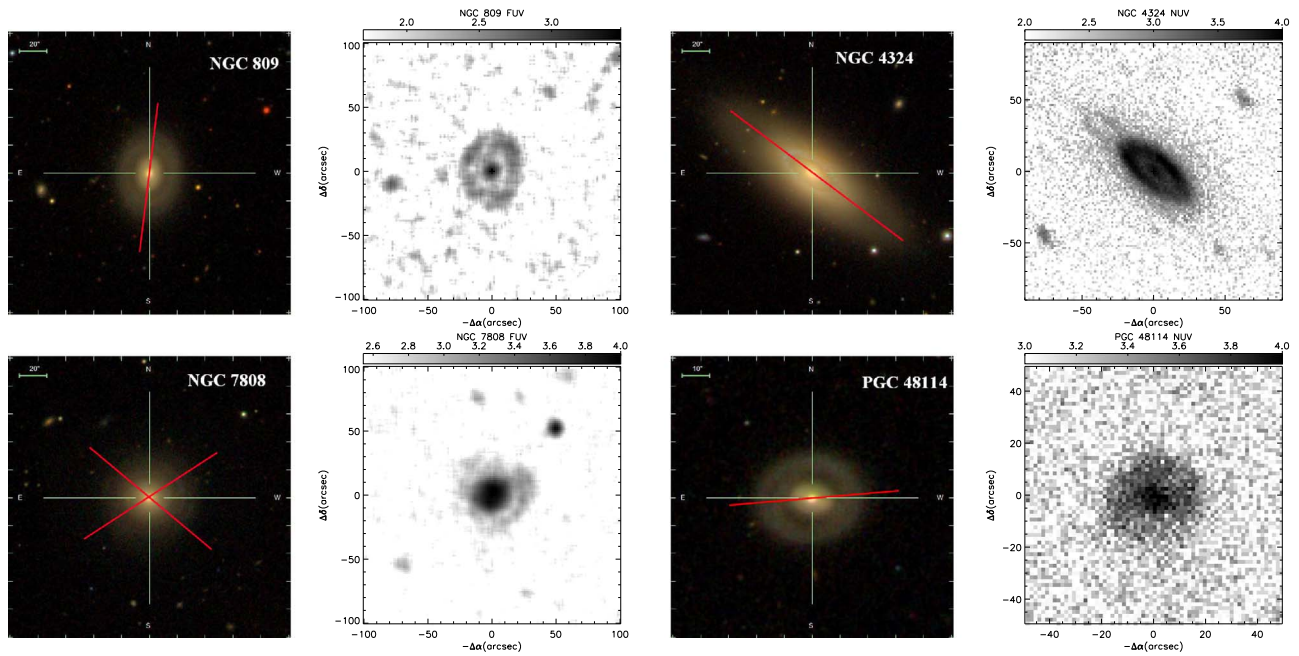


Figure 1. False-color SDSS images of the galaxies under consideration paired with the *GALEX* maps, where the intensities are scaled logarithmically: NGC 809 (upper left), NGC 4324 (upper right), NGC 7808 (bottom left), and PGC 48114 (bottom right). The positions of the spectrograph slit are superposed as red lines.

global properties of the galaxies under consideration are given in Table 1, and the combined-color images of four galaxies taken from the Sloan Digital Sky Survey (SDSS) database are presented in Figure 1. All of the galaxies look like bona fide early-type disk galaxies: without spirals and with a smooth reddish appearance. All of them are classified as unbarred galaxies.

2. Long-slit Spectroscopy

2.1. Observations and Data Reduction

The spectral observations were made in a long-slit mode with the Robert Stobie Spectrograph (RSS; Burgh et al. 2003; Kobulnicky et al. 2003) operating at the Southern African Large Telescope (SALT; Buckley et al. 2006; O’Donoghue et al. 2006); a slit width was $1''.25$. All observational details are given in Table 2. The slit was aligned along the major axis for every galaxy except NGC 7808, which looks face-on. The volume-phase grating PG0900 was used for our program to cover the spectral range of $3760\text{--}6860\text{ \AA}$ with a final reciprocal dispersion of $\approx 0.97\text{ \AA pixel}^{-1}$ and FWHM spectral resolution of 5.5 \AA . The seeing during the observations was in the range of $1''.5\text{--}3''.0$. The RSS pixel scale is $0''.1267$, and the effective field of view is $8'$ along the slit. We used a binning factor of 2 or 4 to give a final spatial sampling of $0''.253$ and $0''.507\text{ pixel}^{-1}$, respectively. Every night, the spectrum of an Ar comparison arc was exposed to calibrate the wavelength scale after each galaxy observation, and spectral flats were observed regularly to correct for pixel-to-pixel variations. Spectrophotometric standard stars were observed during twilights, after the observations of objects, that allowed relative flux calibration of the SALT/RSS spectra.

Primary data reduction was done with the SALT science pipeline (Crawford et al. 2010). After that, the bias- and gain-corrected and mosaicked long-slit data were reduced in the way described in Kniazev et al. (2008). The accuracy of the spectral linearization was checked using the night-sky

lines [O I] $\lambda 5577$ and [O I] $\lambda 6300$; the rms scatter of their wavelengths measured along the slit is 0.04 \AA . Since the diameters of the galaxies do not exceed $3'$, the sky spectra from the slit edges were used to estimate the background during the galaxy exposures.

2.2. Data Analysis

The spectral data have been used to calculate the line-of-sight velocities of the ionized gas in the galaxies along the slit and to estimate the equivalent widths of the emission lines by means of Gaussian multicomponent fitting of the [N II] $\lambda 6548 + \lambda 6583 + \text{H}\alpha(\text{emission}) + \text{H}\alpha(\text{absorption})$ line blend; also, the Gaussian fitting of the individual emission lines H β and [O III] $\lambda 5007$ (and of [S II] $\lambda 6716.4, \lambda 6730.6$, where they are in the spectral range covered by observations, i.e., in NGC 2697 and NGC 4324) was made. For all of the galaxies, we have also determined the line-of-sight velocities of the stellar component by cross-correlating the blue-green part of the spectra ($4050\text{--}5590\text{ \AA}$) with the spectrum of HD 58972, a bright K-giant star. We summed the spectra over radially increasing bins in the peripheral parts of the galaxies to improve the signal-to-noise ratio (S/N) by taking into account the radial galaxy structure (see the next section).

After that, the Lick indices H β , Mgb, Fe5270, and Fe5335 (Faber et al. 1985; Worthey et al. 1994; Worthey & Ottaviani 1997) were calculated in the same bins. The Lick index system includes the equivalent widths of a dozen strong absorption lines in the integrated spectra of stellar populations that allow one to determine stellar population properties, in particular, mean metallicities and ages, by confronting Balmer-line measurements against the metal-line measurements. The calibration of the Lick indices measured with our instrumental setup (spectrograph, grating, and slit width) into the standard index system is described by Katkov et al. (2015). A separate problem is correction of the Lick index H β for the emission that is prominent in all of our sample galaxies. This was

Table 1
Global Parameters of the Sample Galaxies

Galaxy	NGC 809	NGC 2697	NGC 4324	NGC 7808	PGC 48114
Galaxy type (NED ^a)	(R)S0 ⁺ :	SA0 ⁺ (s):	SA(r)0 ⁺	(R')SA0 ⁰	S? (S0 ^b)
Type of a ring	RL... ^c		(L)SA(r)0 ⁺ /E? ^d	PLA.0 ^c	R ₁ R ₂ SAB(l)0 ⁺ ^d
V_r (NED), km s ⁻¹	5367	1824	1665	8787	6984
Distance, ^e Mpc	71	29	27.5	115	99
R_{25}'' (RC3 ^f)	44	55	83	38	20
R_{25} , kpc (RC3+NED)	14.7	7.6	11.1	20.5	9.3
M_B (LEDA)	-20.03	-18.67	-19.75	-21.39	-19.73
M_H (NED)	-23.74	-22.26	-23.64	-24.71	-23.34
($g-r$) (SDSS ^g)	0.77	...	0.74	0.77	0.80
PA _{phot} (LEDA ^b)	173°5	123°	54°5	...	89°
$M(\text{H I})$, 10 ⁸ M_\odot ^h	...	6	17
$M(\text{H}_2)$, 10 ⁸ M_\odot ⁱ	...	4.1	0.9
Environment ^j	1	2	2	2	1
	(625, +1.8)	(10, -0.8, 237)	(23, +2.0, 100)	(7, +0.8, 94)	(159, +1.5)

Notes.

^a NASA/IPAC Extragalactic Database (<http://ned.ipac.caltech.edu>).

^b Lyon-Meudon Extragalactic Database (<http://leda.univ-lyon1.fr>).

^c According to Nair & Abraham (2010).

^d According to Buta (2017).

^e From NED, “cosmology-corrected” option.

^f Third Reference Catalog of Bright Galaxies (de Vaucouleurs et al. 1991).

^g Sloan Digital Sky Survey, Data Release 9 (Ahn et al. 2012).

^h The source of the H I data—Extragalactic Distance Database (<http://edd.ifa.hawaii.edu>).

ⁱ The source of the H₂ data—Alatalo et al. (2013).

^j The environment types derived from HYPERLEDA and NED searching are coded: 1 is a pair member (numbers in parentheses are separation in kpc, magnitude difference), and 2 is a group member (numbers in parentheses are N gal in the group, magnitude difference with the second- (first)-ranked galaxy, and separation with it in kpc).

Table 2
Long-slit Spectroscopy of the Studied Galaxies

Galaxy	Date	Exp. (s)	Binning	Slit (arcsec)	PA (slit) (deg)	Seeing (FWHM, arcsec)
NGC 809	2011 Oct 7	1020 × 3	2 × 2	1.25	173	2.5
NGC 2697	2012 Nov 22	900 × 3	2 × 4	1.25	305	2.2–2.7
	2013 Feb 16	900 × 3	2 × 4	1.25	305	2.7
NGC 4324	2013 Mar 10	800 × 3	2 × 4	1.25	233	3.5
NGC 7808	2012 Dec 2	600 × 3	2 × 4	1.25	50	1.5
	2012 Dec 4	600 × 3	2 × 4	1.25	123	3.5
PGC 48114	2013 Feb 20	600 × 3	2 × 4	1.25	275	2.7–3.2

accomplished through the measurements of the H α emission-line intensity and equivalent widths (Sil'chenko 2006). After deriving the emission-line equivalent widths by means of Gaussian fitting the blend of [N II] λ 6548 + λ 6583 + H α (emission) + H α (absorption), we diagnosed the gas excitation mechanism by calculating the [N II]/H α ratio. If $\log([\text{N II}]\lambda 6583/\text{H}\alpha)$ was less than or equal to -0.3 , we concluded that the gas was excited by young stars (Kauffmann et al. 2003); if it was larger, then the excitation mechanism in the galactic disk was thought to be shock waves (Allen et al. 2008) and/or old hot stars (Binette et al. 1994). In the former case, we calculated the emission-line flux of the H β emission as the H α emission flux divided by 2.85, and, in the latter case, as one-fourth (Stasińska & Sodr  2001).

3. Structure of the Galaxies

Before deriving conclusions from our spectral results, we studied the structure of the galaxies under consideration to be able to attribute the properties of radially resolved stellar populations to the bulges, disks, or rings and lenses if they are present. For four galaxies, we used the SDSS Data Release 9 (DR9) imaging data (Ahn et al. 2012); but for NGC 2697, special observations were made with the telescope network LCO (Brown et al. 2013), since this galaxy is not in the SDSS footprint. In all cases, the SDSS photometric system, *gri*, was used. Figure 2 shows the radial profiles of the isophote parameters and surface brightness azimuthally averaged with the running values of the isophote ellipticities and orientation angles. At the surface brightness profiles, we mark the radius

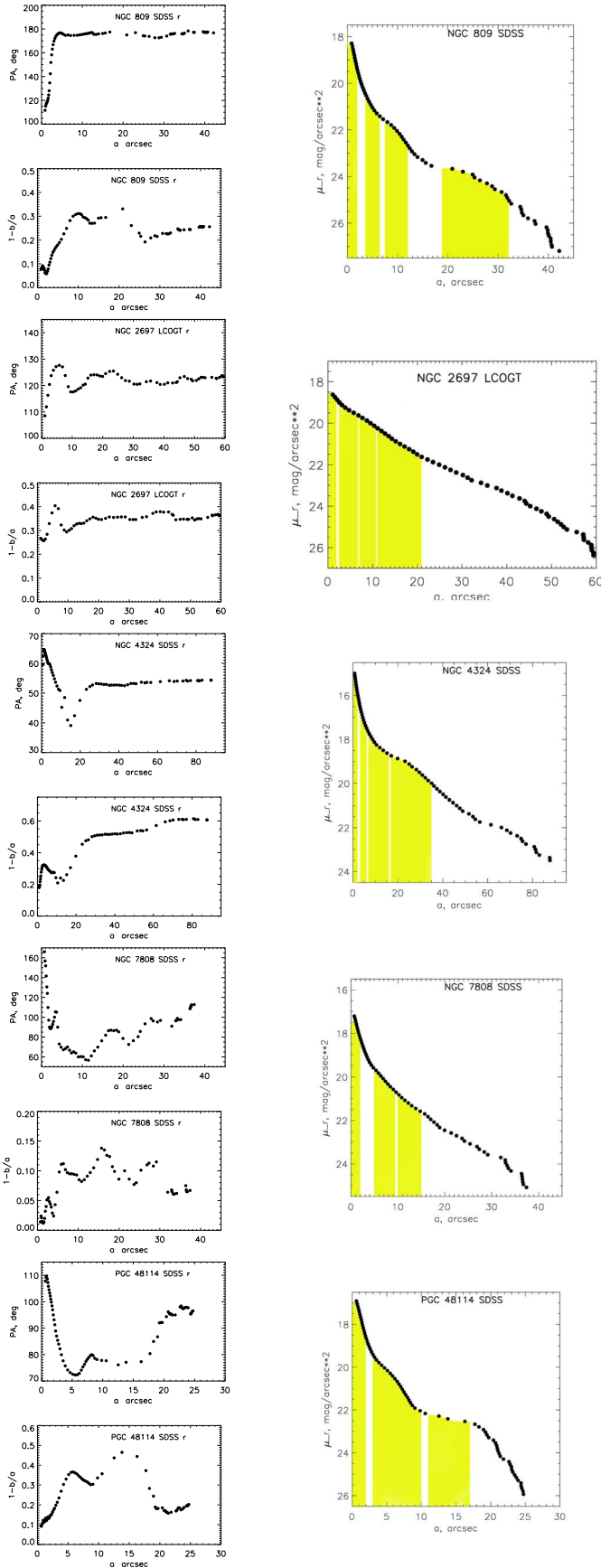


Figure 2. Isophote major-axis PA and ellipticity radial profiles (left) and r -band surface brightness profiles (right). In yellow, we show the radial zones for which the stellar population parameters are studied below.

ranges for which the stellar population characteristics will be analyzed in yellow. Initially, we suggested measuring the stellar population properties in the nuclei, bulges, large-scale stellar disks, and rings. However, we have failed to derive stellar population properties for the bulges in some cases, because NGC 2697 has no classical bulge at all, and in the distant objects NGC 7808 and PGC 48114, our spatial resolution is not sufficient to separate the nuclei and the bulges, the bulges being rather compact. Instead, in some cases, we analyze two radial ranges containing rings, the inner ring being discovered only by inspecting the surface brightness profiles. We stress that here we define the *stellar* rings as seen in the broadband images. The *gaseous* rings marked by intense emission lines are not necessarily exactly coincident with the stellar rings; this will be discussed further in a separate section (Section 5).

In general, four galaxies of the sample look axisymmetric, in accordance with their nominal classification. Only in PGC 48114 are the rings both elliptical, demonstrating local maxima of isophote ellipticity at radii of $6''$ and $15''$ and the isophote major-axis position angle (PA) turn at these radii by some 20° – 25° from the line-of-node orientation. As NGC 7808 is seen nearly face-on, the variations of the isophote major-axis PA in this galaxy could be attributed to the low accuracy of its determination (the isophotes are nearly round). A quite curious feature is found in NGC 4324: at $r = 15''$, just inside the inner ring position at $r = 23''$, the isophotes demonstrate the major-axis turn and the ellipticity minimum. Such isophote behavior may be related to a small bar orthogonal to the line of nodes. However, we think that it is probably not a bar, since no kinematical disturbance of the gaseous disk is observed at this radius.

4. Gaseous and Stellar Rotation

Figure 3 presents line-of-sight velocity profiles for both the stellar and gaseous components in our galaxies. As NGC 2697 was observed twice in the same slit orientation, we present two plots with independent measurements. NGC 7808 was observed in two different slit orientations. But these two cross sections accidentally appear to deviate symmetrically from the line of nodes, and the measured velocity profiles, both for the gas and stars, have coincided perfectly; thus, we present a united plot for this galaxy. In dynamically cold systems, the agreement between the velocity profiles (rotation curves) derived by measuring emission and absorption lines indirectly implies the coincidence of the rotation planes of the stars and ionized gas. The gaseous disks are likely coplanar with the stellar disks in NGC 4324 and PGC 48114. In NGC 2697 and NGC 7808, the stellar component rotates more slowly than the ionized gas, which may indicate that the gaseous disks are tilted with respect to the stellar disks. Alternatively, in the latter galaxy, the difference may be an effect of asymmetric drift because NGC 7808 is the most luminous galaxy in our sample, and we may expect high velocity dispersion in its stellar disk. As for NGC 2697, according to the SAURON data that we have retrieved from the open ING archive, the stellar and ionized-gas components demonstrate very different visible rotation velocities: we see a rotation with a speed less than 80 km s^{-1} in the stellar component and about 200 km s^{-1} for the ionized gas. At a distance of $10''$ – $15''$ from the center, a sharp increase of the stellar velocity dispersion, up to more than

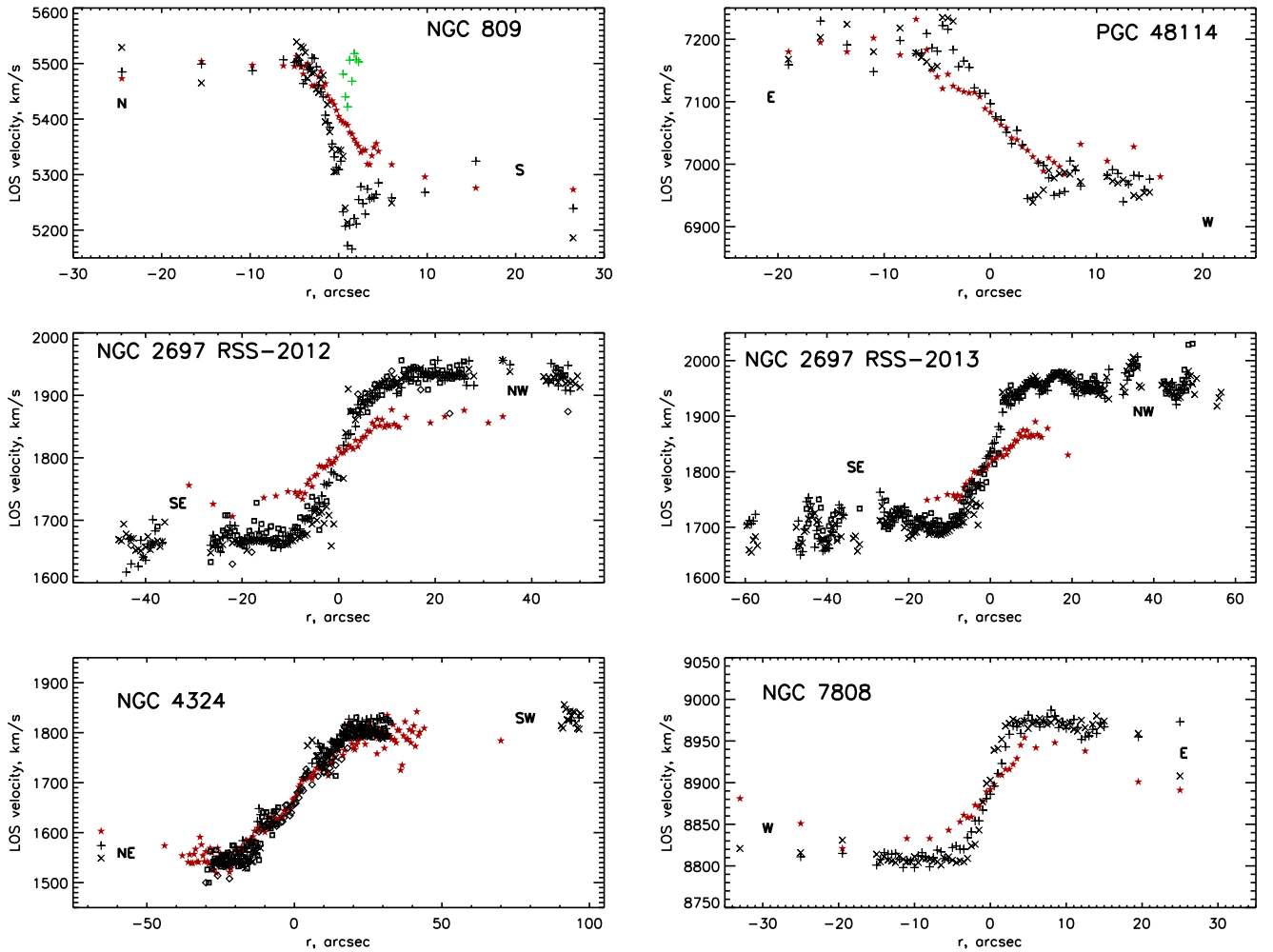


Figure 3. Line-of-sight velocity profiles. Red stars signify stellar rotation, and black symbols refer to the different ionized-gas emission lines: crosses are $H\alpha$, plus signs are $[N II] \lambda 6548 + \lambda 6583$, squares are $[S II] \lambda 6717 + \lambda 6731$, and diamonds are $[O III] \lambda 5007$. For NGC 2697, two independent data sets are presented: those obtained in the same slit orientation in 2012 and in 2013. The emission line $[N II] \lambda 6583$ in NGC 809 shows two components, well separated by their velocities, to the south of the nucleus.

100 km s^{-1} , is observed just at the line of nodes (Figure 4). It is a disk-dominated area (Figure 2), which is expected to be dynamically cold; therefore, we may suspect an overlapping of two kinematically decoupled stellar subsystems along our line of sight—two stellar disks with slightly different inclinations. One of them may be currently forming from freshly accreted gas. But the low spectral resolution of the observations does not allow us to surely state the presence of two kinematically different stellar disks. Also, because of the low spectral resolution, we cannot measure asymmetric drift for the stellar disk in NGC 7808.

In NGC 809, there are apparently strong perturbations in the dynamics of the gaseous disk—we see double-horn profiles of the $[N II]$ emission line just to the south of the nucleus. It may be explained by the possible presence of a compact bar in the central part of this galaxy, which was also implied by the photometric data: the isophote major axis is turned by some 70° within the radius of $5''$. The edges of bars often host shocks betrayed by the dust lanes. If our slit has caught simultaneously shock-excited decelerated gas at the bar edge and freely rotating star-forming gas, we may expect a double-peak emission-line profile reflecting the presence of two kinematically different gaseous subsystems on our line of sight.

5. Excitation and Chemistry of the Ionized Gas

The existence of the prominent emission lines $H\alpha$ and $[N II]$ in the long-slit spectra of the galaxies under consideration, and especially, their good visibility well off the center, are common for all of them. Figures 5 and 6 show the radial profiles of the equivalent widths of the emission lines: $H\alpha$ for four galaxies and $[N II] \lambda 6583$ for NGC 809, where it is the strongest one. One can see that the equivalent widths of the emission lines vary along the radius of the galaxies and show one or more prominent peaks. Presumably, this indicates rings or spirals containing emission-line regions in the gaseous disks of the galaxies. In the spectra of the nearby galaxies NGC 2697 and NGC 4324, we have also detected strong emission lines due to $[S II] \lambda\lambda 6716.4, 6730.6$. For the more distant galaxies, NGC 809, NGC 7808, and PGC 48114, these spectral lines are unfortunately beyond the spectral range of the spectrograph configuration used by us. In the long-slit spectra of NGC 4324, NGC 2697, and NGC 7808, we have also detected the strong emission lines $H\beta$ and $[O III] \lambda 5007$ in the green range seen at the same distances from the center of the galaxies as the emission lines $H\alpha$ and $[N II]$, which makes possible a confrontation between the strong emission-line ratios used for the gas excitation mechanism diagnostics. We have

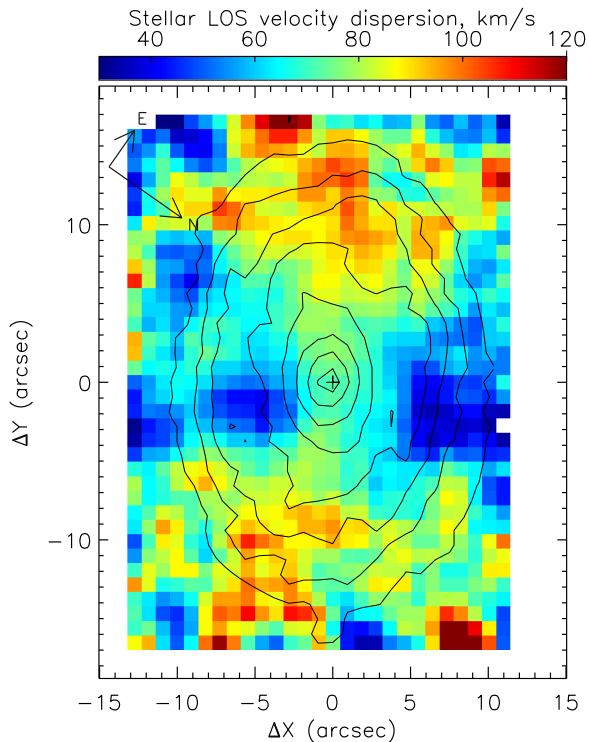


Figure 4. Map of the stellar velocity dispersion for NGC 2697. Two quite untypical features can be seen: the off-center stellar velocity dispersion maxima along the major axis of the disk and the stellar velocity dispersion minima along the minor axis. The latter feature implies the absence of the bulge, and the former one betrays the possible existence of two kinematically decoupled stellar subsystems.

analyzed the relations of the intensities of these emission lines to reveal the excitation mechanism by exploiting Baldwin-Phillips-Terlevich (BPT) diagrams (Baldwin et al. 1981).

To determine the nature of the gas excitation—by young stars or other mechanisms—in the ringlike area of strong emission lines, we have used BPT diagnostic diagrams with the models of Kewley et al. (2001) and the empirical boundaries found by Kauffmann et al. (2003). Figure 7 presents $\log([\text{O III}]/\text{H}\beta)$ versus $\log([\text{N II}]6583/\text{H}\alpha)$ for the galaxies with the full collection of the measured emission lines—NGC 2697 ($r = 16''\text{--}46''$), NGC 4324 ($r = 20''\text{--}26''$), and NGC 7808 ($r = 10''\text{--}14''$). The point clouds are within the area characterized by the gas excitation by young stars (NGC 2697) and the transition zone characterized by the mixing excitation by young stars and shock waves (NGC 4324 and NGC 7808). In NGC 4324, we see the systematic trends of the line intensity ratios between the inner and outer edges of the ring on one hand and its middle line on the other hand. For both the northern and southern cross-points, we have connected three measurements, those at $r = 20''$, $22.5''$, and $25''$, and plotted them at the BPT diagram. In Figure 7, one can see that the middle measurements at both the northern and southern tip of the ring are the closest to the line dividing H II region excitation and the transition zone. So, we may suspect that the ring in NGC 4324 is dynamically compressed by the ambient medium producing shock fronts at its edges.

By adopting the restrictions on the line intensity ratios from Kewley et al. (2006), we suggest that the N2 ratio $\log([\text{N II}]6583/\text{H}\alpha) \leq -0.3$ signifies the gas excitation by young stars in any case. Figure 8 traces the ratios, $\log([\text{N II}]6583/\text{H}\alpha)$,

along the radius of the galaxies. In PGC 48114, only the western half of the disk demonstrates the coincidence of the sharp peak of the emission-line intensity and of the $\log([\text{N II}]6583/\text{H}\alpha)$ ratio typical for star formation, at $r \approx +13''$. In NGC 809, the emission-line ratio $[\text{N II}]6583/\text{H}\alpha$ is everywhere larger than 1, so in this galaxy, despite the gas presence and the bright UV ring (Figure 1), we do not see any signs of current, $T < 30$ Myr, star formation in the ring.

The strong line intensity ratios are used by us to estimate the physical and chemical characteristics of the gas. The relation of two lines of the sulfur doublet, $[\text{S II}]6716.4/[\text{S II}]6730.6$, allows us to estimate the electron density in the ionized gas by using the calibration of Osterbrock & Ferland (2006). To derive oxygen abundances for the regions where the gas excitation is dominated by the star formation process, we have used quite recent strong line calibrations by Marino et al. (2013); two different indicators, O3N2 and N2, are exploited. The results are presented in Table 3 (the radius ranges correspond to the intensity peaks of the emission lines in the disks). The gas metallicity in the star-forming rings of the galaxies under consideration looks homogeneous and only slightly subsolar, being everywhere higher than the stellar metallicity of the underlying galactic disks, which is commonly less than half solar (see the next section).

6. Stellar Populations

To estimate stellar population properties in different parts of the galaxies, we have measured the Lick indices ($\text{H}\beta$, Mgb , Fe5270 , and Fe5335) along the slit, which is mostly aligned with the major axes. Since the galaxies reveal emission lines in their spectra at some radii, their stellar Lick indices $\text{H}\beta$ are contaminated by the Balmer emission line of the ionized hydrogen. The equivalent widths of the $\text{H}\alpha$ emission line derived by us from the red-range spectra were used to calculate the correction for the $\text{H}\beta$ index. The $\text{H}\beta$ emission-line intensities are related to the $\text{H}\alpha$ emission-line intensities through the Balmer decrement, which depends on the ionization model under the assumption of the hydrogen excitation mechanism. We have used BPT diagnostic diagrams (see the previous section) to determine the nature of the excitation mechanism (by young stars or due to other reasons), accept some model-based Balmer decrement, and calculate the $\text{H}\beta$ index correction. In any case, $\Delta\text{H}\beta \leq 0.35 \text{EW}(\text{H}\alpha \text{ emission})$; the lowest Balmer decrement, $\text{H}\alpha/\text{H}\beta = 2.85$, characterizes the H II region-like excitation.

After correcting the $\text{H}\beta$, we compared the measured Lick indices to the models of simple stellar populations (SSPs) by Thomas et al. (2003) to determine mean stellar population properties, such as SSP-equivalent ages, metallicities, and magnesium-to-iron abundance ratios. The models by Thomas et al. (2003) are calculated for several values of $[\text{Mg}/\text{Fe}]$. It allows us to determine magnesium-to-iron abundance ratios for the stellar populations over the different parts of the galaxies and to estimate the duration of the last major star-forming episode. Chemical evolution models suggest the difference in the timescales of iron and magnesium production by a single stellar generation. Brief star formation, $\Delta T < 1$ Gyr, would give a significant magnesium overabundance up to $[\text{Mg}/\text{Fe}] = +0.3$ to $+0.5$, and only continuous star formation during more than 2–3 Gyr provides the solar Mg/Fe abundance ratio (Matteucci & Greggio 1986).

In Figure 9, we show the Lick indices profiles along the major axes of the galaxies plotted onto diagnostic diagrams

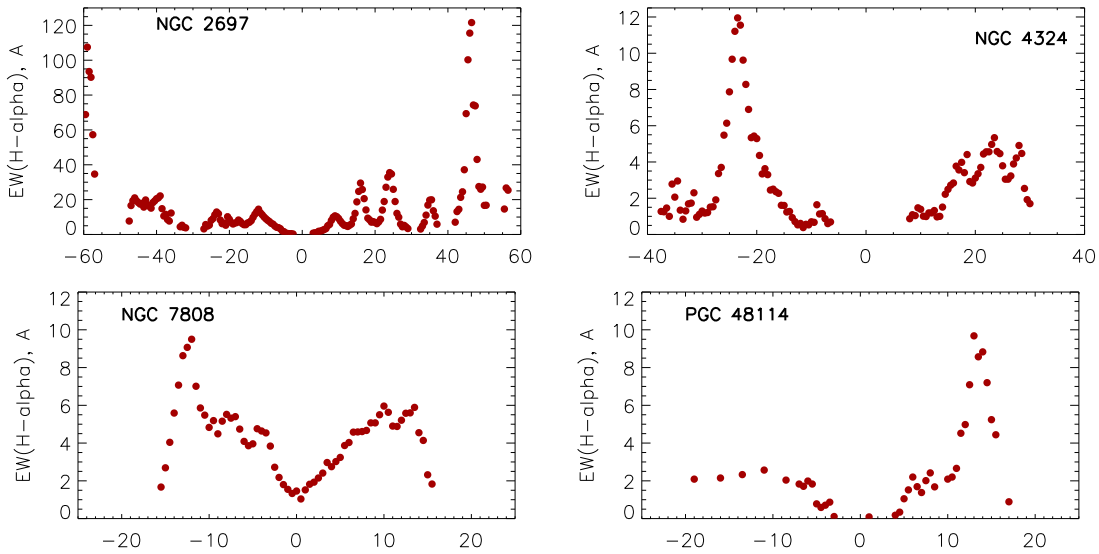


Figure 5. Emission-line equivalent width radial cutoff: star-forming rings seen in the $H\alpha$ emission line.

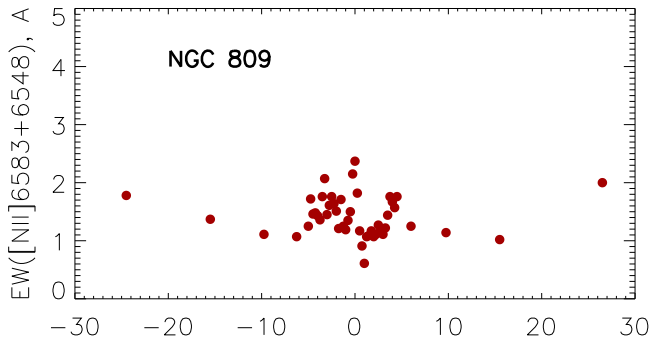


Figure 6. The [N II] emission-line intensity profile in NGC 809.

$\langle \text{Fe} \rangle = (\text{Fe}5270 + \text{Fe}5335)/2$ versus Mgb and $H\beta$ versus $[\text{MgFe}] \equiv \sqrt{\text{Mgb}\langle \text{Fe} \rangle}$. With these diagrams, we can trace the mean ages, metallicities, and magnesium-to-iron ratios along the radius in every galaxy studied. In general, we can note that in all five galaxies, the central stellar populations are of intermediate age, 5–8 Gyr, and have solar or supersolar metallicity, while no current or even recent star formation is detected in the nuclei and bulges. The star formation histories in their stellar disks are rather different, but everywhere the mean stellar metallicities in the disks including the stellar rings are below $[Z/H] \sim -0.3$.

7. Discussion

The current paradigm of the evolution of disk galaxies implies persistent accretion of outer cold gas onto disks that provides, e.g., the flat relation between the ages and metallicities of disk stars in our Galaxy and also continuous star formation within galactic thin disks of other spiral galaxies during the last 8–10 Gyr, despite the current supply of the gas in the disks being sufficient for only ~ 2 Gyr of star formation with the rate observed. Interestingly, the timescale of gas consumption, 2 Gyr, is nearly constant for the disks of nearby spirals (Bigiel et al. 2011), and this fact has inspired suggestions that galactic star-forming disks are now in equilibrium (Davé et al. 2012): the rate of outer gas accretion is nearly equal to the star formation rate (SFR) plus gas outflow in so-called “galactic fountains” due to star formation feedback.

In the frame of this paradigm, all of the gas currently observed in the disks of spiral galaxies must be recently accreted from outside; no gas can be considered as a primordial aspect. If correct, there must be no general difference between the well-settled gaseous disks of spiral galaxies and the (often) inclined gaseous disks of lenticulars. We may expect to find star formation in lenticular galaxies with noticeable gas content. Pogge & Eskridge (1987, 1993) searched for H II regions in gas-rich S0s and found them in only half of the sample studied. Two subsamples, with and without star formation, showed similar mean HI content, contradicting, at first glance, the Kennicutt–Schmidt prescription that the SFR has to be proportional to the gas mass. The cause of star formation suppression in half of the gas-rich S0s remained unclear. However, the galaxies that we have studied in this work were selected through the UV ring visibility criterion, and indeed, just four of the five galaxies reveal currently star-forming regions detected through the intense $H\alpha$ emission line. Here we consider the S0s from the first half, in the terms by Pogge and Eskridge.

7.1. SFR in the S0 Rings

We can determine the integrated SFRs evidently related to the rings in these particular galaxies by using the FUV magnitudes measured by *GALEX* and listed in the NASA/IPAC Extragalactic Database (NED; <http://ned.ipac.caltech.edu>). We have taken the calibration of the SFR through the *GALEX* FUV magnitudes from the work by Lee et al. (2011). The integrated FUV magnitudes listed in the NED were corrected for the foreground extinction but not for the intrinsic dust of the lenticular galaxies under consideration. For NGC 809 and NGC 7808, we have taken “asymptotic” FUV magnitudes from the recent compilation by Bai et al. (2015); these FUV magnitudes are more luminous by 0.1–0.3 mag than the data in the NED. The calculated estimates of the SFRs (over the timescale of 100 Myr) for three galaxies are between $0.1 M_{\odot} \text{yr}^{-1}$ (PGC 48114 and NGC 4324) and $0.2 M_{\odot} \text{yr}^{-1}$ (NGC 2697); NGC 7808 appears to be rather intensely forming stars, with $\text{SFR} = 1 M_{\odot} \text{yr}^{-1}$. We have found a few similar luminous S0 galaxies with an SFR of about $1 M_{\odot} \text{yr}^{-1}$ in the SDSS sample by Nair & Abraham (2010)—for example, the

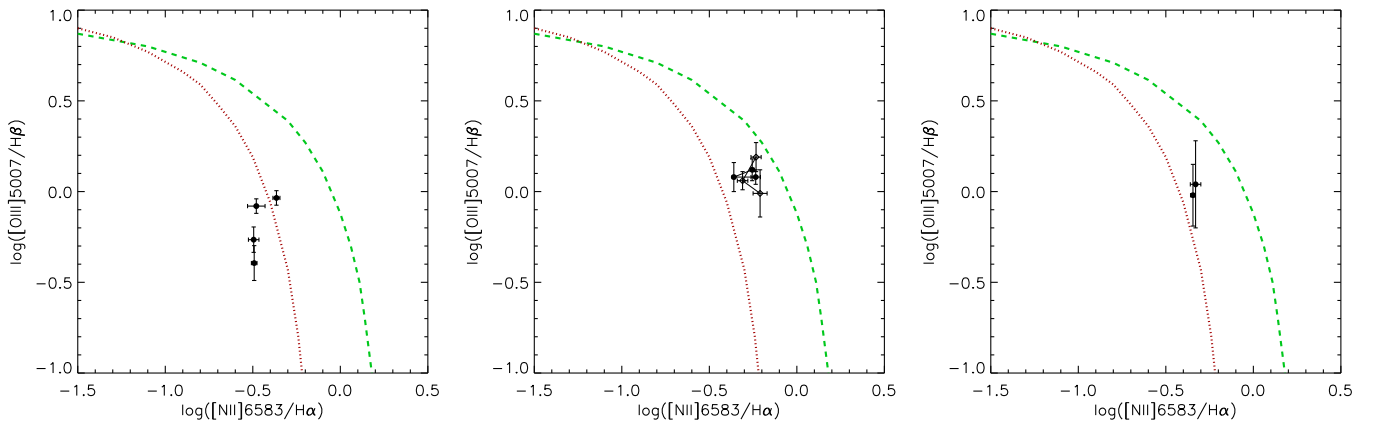


Figure 7. The BPT diagrams for the emission-line rings in NGC 2697 (left), NGC 4324 (middle), and NGC 7808 (right). The green dashed line marks the theoretical border of star formation excitation from Kewley et al. (2001), and the red dotted line is the empirical boundary between star-forming galactic nuclei in SDSS and other types of nuclear emission excitation from Kauffmann et al. (2003). For NGC 4324, we show the radial cuts through the ring (points connected by solid lines): the middle of the ring demonstrates the excitation that is the closest to the H II region one.

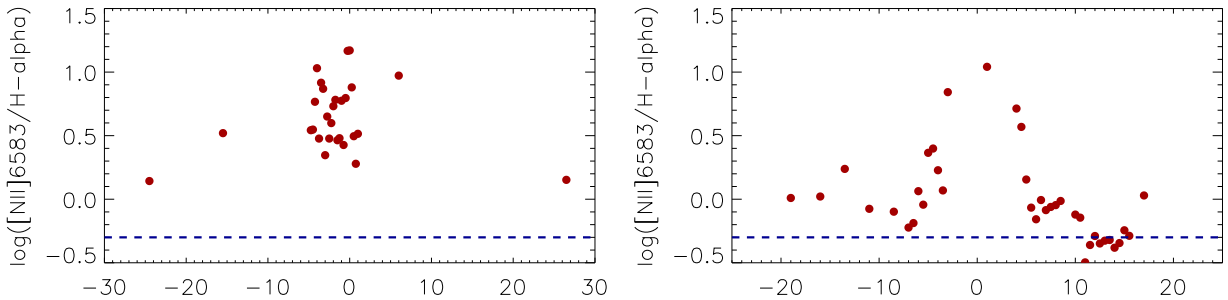


Figure 8. Profiles of emission-line intensity ratios for NGC 809 (left) and PGC 48114 (right). The horizontal dashed line divides the area occupied by the spectral characteristics of the ionized gas excited by young stars (below the line) and other mechanisms of gas excitation (above the line).

unbarred central group S0 PGC 36834 resembles NGC 7808 very much. In general, such a level of star formation puts all four S0s close to the “main sequence”—in particular, within the scaling relation between the integrated SFR and blue absolute magnitude for star-forming galaxies of Sa–Sc type by Bothwell et al. (2009). With its $\text{SFR} = 0.066 M_{\odot} \text{ yr}^{-1}$, NGC 809 falls slightly below the boundaries of the “main sequence,” and it is the only galaxy of our sample where the UV-bright ring shows no emission-line spectrum excited by young stars. For NGC 2697 and NGC 4324, there are measurements of the gas content of both the neutral hydrogen (the data in Table 1 are taken from the Extragalactic Distance Database, <http://edd.ifa.hawaii.edu>) and the molecular gas (Alatalo et al. 2013). With the SFR estimates obtained above, the molecular gas consumption times are 2.1 Gyr for NGC 2697 and 800 Myr for NGC 4324, the latter being shorter than the typical 2 Gyr for spiral galaxies (Bigiel et al. 2011). The HI consumption times, 3 Gyr for NGC 2697 and 14 Gyr for NGC 4324, are quite typical (Bothwell et al. 2009). The general impression is that NGC 2697 and NGC 4324 have normal (for their masses) HI content and SFR (Bothwell et al. 2009). Nevertheless, they are not spirals, they are lenticulars, and their star formation is assembled into the UV-bright rings.

In fact, we have in hand three independent indicators of the SFR: two *GALEX*-measured fluxes, those in the NUV band and FUV band, and also the $\text{H}\alpha$ emission-line intensity. For the latter, we have converted the fluxes into the absolute energy units by normalizing the red continuum measured over the galactic spectra along the slit to the known photometric r -band

surface brightness profiles (Figure 2). These three indicators probe the SFR over different timescales—the NUV flux over the last 200 Myr, the FUV flux over the last 100 Myr—and the $\text{H}\alpha$ emission produced by the Stromgren zones around massive stars provides the current SFR, since stars with masses larger than $10 M_{\odot}$ possessing Stromgren zones live no more than 10–20 Myr (Kennicutt & Evans 2012). By comparing the SFR estimates made by using three different indicators, we can determine the qualitative trends of the star formation histories. We have cut the *GALEX* images of our galaxies with digital slits applying the slit characteristics given in Table 2 for every galaxy, converted the *GALEX* counts into the energy units by using the recommendations from Morrissey et al. (2007), determined the NUV- and FUV-based SFRs by using the formulae from Kennicutt & Evans (2012), and corrected them for the intrinsic dust by using *WISE* 22 μm images. The current SFRs have been determined from the $\text{H}\alpha$ emission-line fluxes by also using the formulae from Kennicutt & Evans (2012). After that, we have divided the SFRs obtained by the areas covered by the slit and, in such a way, derived the local SFR surface density in the rings. These estimates are plotted in Figure 10 for four rings in three galaxies. Almost all of the star formation histories behave similarly: they fall with time over a timescale of some 10^8 yr. Only the NE tip of the NGC 4324 ring demonstrates the quite recent start of the local star formation (the $\text{H}\alpha$ -estimated SFR exceeds those derived from the UV fluxes)—in this galaxy, the star formation is very inhomogeneous along the ring. By fitting three SFR ticks for every ring with a straight line, we have roughly estimated the e -

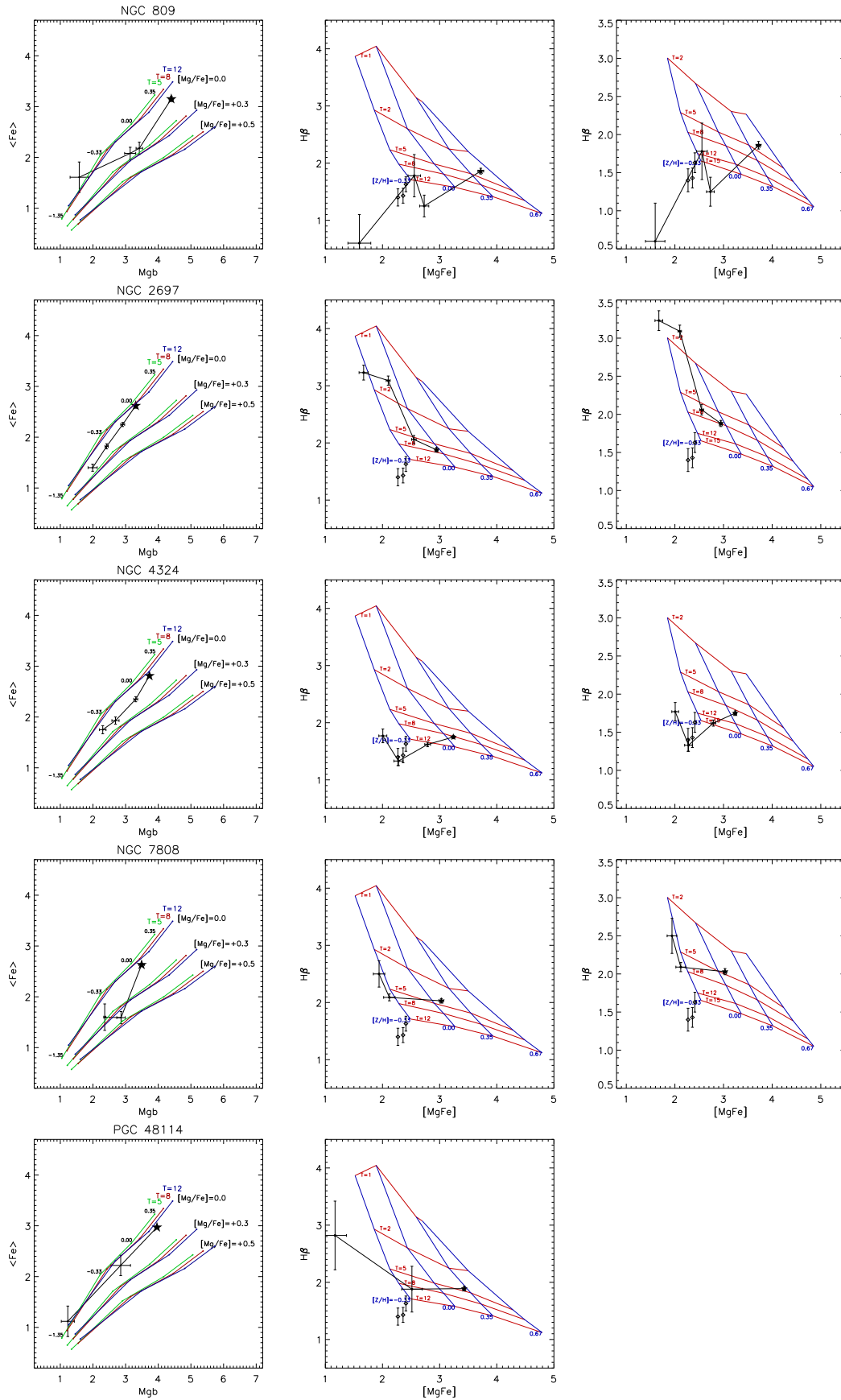


Figure 9. Diagnostic diagrams to determine the SSP-equivalent parameters of the stellar populations. The left column presents the $\langle \text{Fe} \rangle = (\text{Fe}5270 + \text{Fe}5335)/2$ vs. Mgb diagram, and the other two columns present the $H\beta$ vs. $[\text{MgFe}] = (\text{Mgb}(\text{Fe}))^{1/2}$ diagrams for $[\text{Mg}/\text{Fe}] = 0$ (middle) and $[\text{Mg}/\text{Fe}] = +0.3$ (right). Large black stars mark the nucleus for every galaxy, and then we go along the radius through the zones described in the section devoted to the structure of the galaxies. The diamonds present a few globular clusters from Beasley et al. (2004) belonging to the Galactic bulge as the reference frame.

Table 3
Ionized-gas and Star Properties of the Rings in the Studied Galaxies

Galaxy	Radius	$\langle N_e \rangle$, cm ⁻³	Gas [O/H] (O3N2)	Gas [O/H] (N2)	[Z/H](stars)
NGC 2697	+16''	100–250	-0.145 ± 0.04	-0.19 ± 0.05	-0.4
	+24''	100–250	-0.15 ± 0.03	-0.18 ± 0.05	
	+46''	<60	-0.21 ± 0.03	-0.19 ± 0.05	
NGC 4324	-23''	100	-0.26 ± 0.03	-0.11 ± 0.04	-0.5
	+94''			-0.18 ± 0.06	
NGC 7808	-24''			-0.15 ± 0.03	
	-12''		-0.24 ± 0.07	-0.11 ± 0.04	-0.4
	+12''		-0.24 ± 0.02	-0.12 ± 0.01	-0.4
PGC 48114	+13''			-0.105 ± 0.04	-1.0

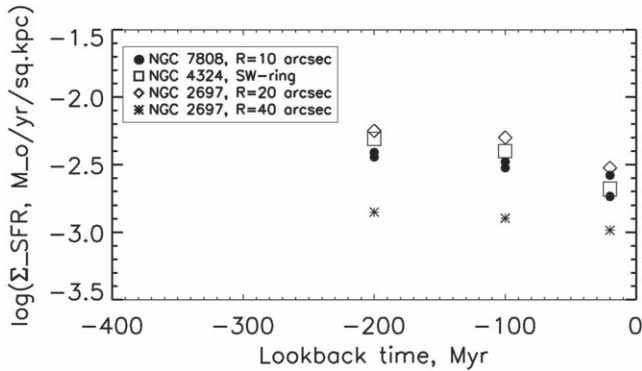


Figure 10. Recent star formation histories in the rings of NGC 7808, NGC 2697, and NGC 4324. For NGC 7808, both its spectral cross sections, in PA = 50° and 123°, are plotted separately.

folding times of the SFR decline; these timescales appeared to be mostly in the range of 200–350 Myr, with a stand-alone e -folding time of 600 Myr in the outer ring of NGC 2697 that is much shorter than typical SFR e -folding times in the disks of spiral galaxies. Note that it is an upper limit of the e -folding times, because if star formation has started more recently than 200 Myr ago, the NUV-based estimate of the SFR must be increased, and the points at $T = 200$ Myr in Figure 10 must be shifted to later times, both corrections making the SFR decline steeper.

7.2. Chemical Evolution of the Star-forming Rings in S0s

By using strong line calibrations, we have determined the gas metallicities in the star-forming rings and compared them with the stellar metallicities of the underlying disks. One can see in Table 3 that the gas metallicities in all four galaxies with intense star formation in the rings are tightly grouped around $[O/H] = -0.1 \dots -0.2$ dex. This is based on the recent calibrations by Marino et al. (2013). If we use the most popular calibration by Pettini & Pagel (2004), we obtain a strictly solar oxygen abundance. This is not the first hint that the star-forming gas in S0s is of homogeneously solar metallicity. We have measured solar gas metallicities in the rings of NGC 6534 and MCG 11-22-015 (Sil'chenko et al. 2018). Ilyina et al. (2014) obtained just such metallicities for the star-forming rings of S0 galaxies NGC 252 and NGC 4513. Much earlier, Pogge & Eskridge (1999), in their survey of H II regions in gas-rich S0s, noted that in all six galaxies with spectra of sufficient quality, the oxygen abundance of the

ionized gas was solar, including two galaxies with counter-rotating (and so evidently accreted!) gaseous disks. Now we also know that the underlying stellar disks have lower metallicity (Table 3).

Some recent models of gas chemical evolution in disks of spiral galaxies, which include persistent gas inflow and outflow (e.g., Kudritzki et al. 2015), show that the gas oxygen abundance rather quickly reaches some asymptotic enrichment level close to the solar metallicity. The timescale of this process is below but close to the gas consumption time (Lilly et al. 2013). Our finding of the homogeneously solar oxygen abundance in the gas of the star-forming rings of lenticular galaxies is consistent with their accretion origin: pure gas accretion, over period of a few hundred Myr, with a rate of order of, say, half of the SFR, provides the asymptotic oxygen abundance of the ionized gas within the star-forming rings just after depletion of half of the gas supply (Kudritzki et al. 2015). With our e -folding times of 200–350 Myr, it means that the current gas oxygen abundance observed is reached after only 150–200 Myr of continuous star formation.

7.3. Gas Origin

The origin of the accreted gas remains vague. Its metallicity is close to solar, though we observe the outer parts of the galactic disks. There is a well-elaborated idea that the gas feeding star formation in the disks of spiral galaxies represents cooling gas from the halo coming into the disks with galactic fountains returning after blowing out from the star-forming sites (Marinacci et al. 2010). Since in this case, the gas clouds leaving the central parts of the disks fall to the outer disk regions following ballistic orbits (Fraternali & Binney 2006), we can expect that in the outer rings, we can meet the gas pre-enriched close to the galactic centers; commonly known negative metallicity gradients in the disks of spiral galaxies serve well for this. However, the estimated timescale of galactic fountain return into the disks is less than 10^8 yr (e.g., Houck & Bregman 1990), so to involve such a mechanism of accretion, we need recent star formation in the central parts of our galaxies. In contrast, all of our galaxies have central stellar populations older than 4 Gyr. In our particular case of the S0 galaxies without recent star formation in the centers, the mechanism of their own gas re-accretion through galactic fountains seems improbable.

Our galaxies belong to the “field”; their environments are not very dense. Only NGC 4324 may be ascribed to the outskirts of

the Virgo cluster. None of those demonstrate any signs of interaction. In view of this, possible sources of the gas accretion may be filaments of the large-scale universe structure or minor merging with gas-rich satellites. In fact, these two mechanisms may play concurrently. In NGC 809 and PGC 48114, where the rings are well seen in the UV and are detached from the main bodies of the galaxies in the optical bands, we have found a significant difference of the stellar population properties between the rings and the inner parts of the galaxies: the rings demonstrate solar magnesium-to-iron ratios and very low stellar metallicity, $[Z/H] \approx -1$, unlike supersolar Mg/Fe and metallicity at the level of half solar in the usual disks of lenticular galaxies (Sil'chenko et al. 2012). We may suggest that both the gas and a major part of the stars in the rings of these two galaxies have an external origin, and the most probable source of the accretion seems to be a late-type satellite merging from a high-momentum orbit. In the other three galaxies, NGC 2697, NGC 4324, and NGC 7808, the UV rings are embedded into their large-scale stellar disks, and the only certain difference between the stellar populations of their rings and the surrounding stellar disks is a systematically lower mean stellar age in the former that is not astonishing when taking into account the current star formation localized just within the rings. In these cases, outer cold gas accretion from filaments is a reasonable interpretation because the rather intense star formation in the rings for a few hundred Myr is able to increase the gas metallicity toward the nearly solar value even from a very low initial level. However, the accretion events might occur only less than 1 Gyr ago, and it is a special challenge to invent a scenario of a galaxy group dynamical evolution that would provide sporadic gas accretion from a cosmological filament onto the early-type group members at particular moments long after the group assembled.

8. Conclusions

We have spectrally studied five lenticular galaxies with UV-bright outer rings. Four of the five rings are also bright in the H α emission line, and the spectra of the gaseous rings extracted around the maxima of the H α equivalent width reveal excitation by young stars, betraying current star formation in the rings. The integrated level of this star formation is $0.1\text{--}0.2 M_{\odot} \text{ yr}^{-1}$, with an outstanding value of $1 M_{\odot} \text{ yr}^{-1}$ in NGC 7808, that is within the “main sequence” of nearby star-forming galaxies. However, the difference in chemical composition between the ionized gas of the rings and the underlying stellar disks that are metal-poor implies a star formation burst within a lookback time of less than 1 Gyr induced by recent accretion of gas or another possible impact event (e.g., infall of a small gas-rich satellite).

The study of the outer rings in disk galaxies has been supported by grant No. 18-02-00094a of the Russian Foundation for Basic Researches. The study is based on the observations made with the Southern African Large Telescope (SALT), programs 2011-3-RSA_OTH-001, 2012-1-RSA_OTH-002, and 2012-2-RSA_OTH-002. A.Y.K. acknowledges support from the National Research Foundation (NRF) of South Africa. This research has made use of the NASA/IPAC Extragalactic Database (NED), which is operated by the Jet Propulsion Laboratory, California Institute of Technology, under contract with the National Aeronautics and Space Administration, and of the Lyon Extragalactic Database (HyperLEDA; <http://leda.univ-lyon1.fr>). In this study, we used the SDSS DR9 data (<http://www.sdss3.org>). Funding for the

SDSS and SDSS-II has been provided by the Alfred P. Sloan Foundation, the Participating Institutions, the National Science Foundation, the U.S. Department of Energy, the National Aeronautics and Space Administration, the Japanese Monbukagakusho, the Max Planck Society, and the Higher Education Funding Council for England. To estimate the star formation rates in the galactic rings, we have used public archive data of the space experiments *GALEX* and *WISE*. The NASA *GALEX* mission data were taken from the Mikulski Archive for Space Telescopes (MAST). The STScI is operated by the Association of Universities for Research in Astronomy, Inc., under NASA contract NAS5-26555. The *WISE* data exploited by us were retrieved from the NASA/IPAC Infrared Science Archive, which is operated by the Jet Propulsion Laboratory, California Institute of Technology, under contract with the National Aeronautics and Space Administration. This paper makes use of data obtained from the Isaac Newton Group Archive, which is maintained as part of the CASU Astronomical Data Centre at the Institute of Astronomy, Cambridge.

This paper is dedicated to our colleague who did much to study the rings in galaxies—to Ira Kostiuk, who passed away suddenly at the end of this April.

Facilities: SALT(RSS), LCOGT, SDSS, GALEX, WISE, NED.

Appendix Notes on the Individual Galaxies

NGC 809. In NGC 809, we inspect the nucleus, bulge, and two rings—the inner one, purely stellar and red, at $r = 10''$ (3.5 kpc), and the outer one, at $r = 19''\text{--}32''$ (Ilyina & Sil'chenko 2011), demonstrating the prominent UV signal (Figure 1) that may also be classified as a pseudo-ring. In the meantime, in the outer ring, the stellar population is older than 15 Gyr (Figure 9); the relative abundance of α -elements is close to the solar value, and the stellar metallicity falls to $[Z/H] \sim -1$, both facts pointing at continuous ineffective star formation, which is typical, for example, for dwarf galaxies. The stellar population of the inner galaxy in the area in the range $3'' < r < 19''$ demonstrates the following properties: the mean age is 15 Gyr, the metallicity $[Z/H] \sim -0.3$, and the abundance ratio $[Mg/Fe] \approx +0.3$, which implies a brief ancient star formation epoch in the main disk of the galaxy. The strong difference between the chemical properties of the outer stellar ring and the rest of the (inner) galaxy, together with the detached outer ring seen in all photometric bands (Figure 1), implies possible accretion of a small satellite with high orbital momentum onto the outer part of NGC 809. Another minor merging with a gas-rich satellite could lead to a prolonged effective star formation episode in the central part of the galaxy ($r < 3''$) that had stopped about 3.5–5 Gyr ago and then rejuvenated the stellar population of the galactic center. As a result, in the nucleus of NGC 809, the mean age of the stellar population is 4–5 Gyr, the metallicity $[Z/H] \sim +0.5$, and the ratio $[Mg/Fe] = +0.1$. One can see that in the center, the relative abundance of α -elements is lower than the one in the disk of the galaxy but slightly exceeds the solar value, because all of the iron from the last starburst did not have time to come into the last generation of the newly born stars before the star formation ceased.

NGC 2697. In NGC 2697, we recognize the nucleus, the circumnuclear dust (red) ring at $r = 3''\text{--}7''$ (Figure 11), the inner UV ring at $r = 7''\text{--}11''$ (Figure 11), and a regular stellar disk between $r = 11''$ and $21''$. The galaxy has no classical bulge (see Figure 2, the surface brightness profile of

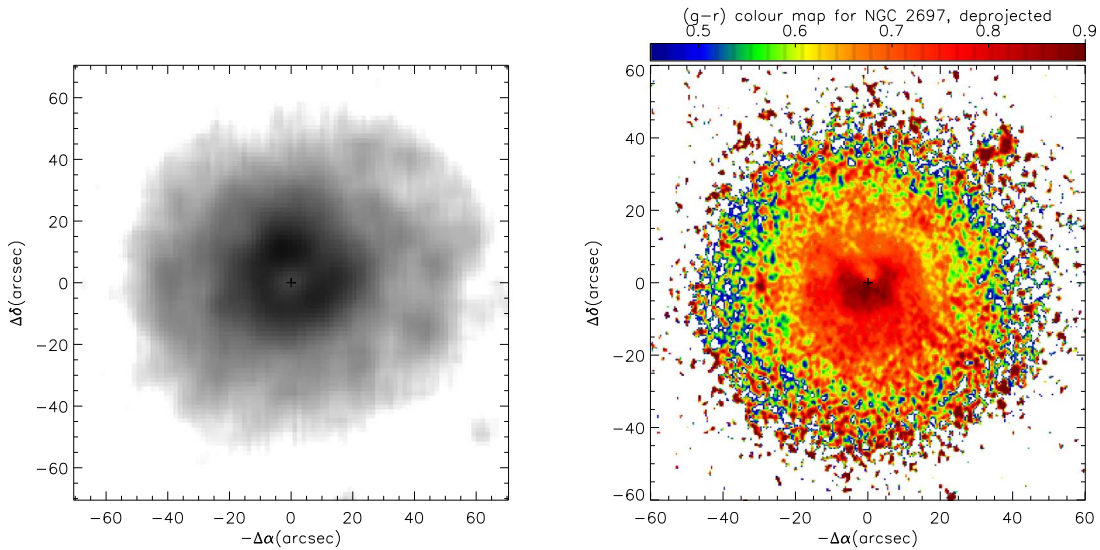


Figure 11. Deprojected maps for NGC 2697. We have turned the initial images by $\sim 30^\circ$ to put the line of nodes horizontally and then stretched them in the vertical direction to take into account the disk inclination of 60° implied by the continuum isophote ellipticity. The *GALEX* FUV image (left) reveals a bright, round ring with $r \approx 9''$ and a clumpy, elliptical decentered ring at $r \approx 40''$. The $(g-r)$ deprojected map derived from our LCO observations demonstrates a circumnuclear dust ring with a radius of about $5''$ (right).

NGC 2697), but at a distance of $7''$ – $10''$ from the center, the low-contrast inner stellar ring can be detected in the r band. It is also the location of the UV ring in this galaxy, and just starting from this radius, we observe strong emission lines excited by young stars. At distances of $r > 7''$ from the center, the stellar population is rather young, with a mean age of 1.5 Gyr and a relative abundance of α -elements $[\text{Mg}/\text{Fe}] \approx +0.2$ to $+0.3$. A prominent metallicity gradient is observed in the stellar component, from $[\text{Z}/\text{H}] \sim -0.1$ at the radii of $7'' < r < 11''$ to $[\text{Z}/\text{H}] < -0.33$ at the radii of $11'' \leq r < 21''$. In the inner part of the galaxy ($2'' < r \leq 7''$), the mean (SSP-equivalent) age of the stellar population is 5–7 Gyr, the abundance ratio $[\text{Mg}/\text{Fe}] \approx +0.1$, and the metallicity $[\text{Z}/\text{H}] \approx -0.2$. In the center ($r \leq 2''$), the mean age of the stellar population is 7 Gyr, and the abundance ratio, as well as the total metallicity, is close to the solar value that points at continuous effective star formation in the central part of the galaxy. With its negative metallicity and age gradients, NGC 2697 supports the idea of “inside-out” disk formation in accordance with the classical paradigm (Fall & Efstathiou 1980; Chiappini et al. 1997). This implies that star formation began in the galactic center and ceased there about 7 Gyr ago, then proceeded farther from the center, in the region $2'' < r \leq 7''$, where it was inefficient and ceased about 2.5–4 Gyr ago (for the connection between the SSP-equivalent age and the age of star formation quenching, see, e.g., Smith et al. 2009). After that, there was a pause in the star-forming process. Presumably, about 1.5 Gyr ago, a dwarf galaxy merged with NGC 2697, a process that added metal-poor stars to the outer parts of the galaxy, ignited intense star formation in the inner disk of the galaxy, and caused a series of brief starbursts organized like rings that we are still observing presently as a clumpy pattern of the disk. Furthermore, the gas has nearly solar metallicity just where the emission lines are excited by the star-forming process.

NGC 4324. In NGC 4324, we investigate the nucleus, bulge, roundish lens between $r = 7''$ and $16''$, and UV ring area. In Figure 9, one can see that in the center ($r \leq 3''$) of NGC 4324, the mean age of the stellar population is about 8 Gyr, the



abundance ratio is close to the solar value, $[\text{Mg}/\text{Fe}] \geq 0$, and the metallicity is slightly supersolar, $[\text{Z}/\text{H}] \sim +0.1$, which points at continuous effective star formation in the nucleus of the galaxy. At the radii of $3''5 \leq r \leq 6''$ from the center, in the bulge-dominated area, the mean age of the stellar population is about 13 Gyr, the abundance ratio rises to $[\text{Mg}/\text{Fe}] = +0.15$, and the metallicity decreases to $[\text{Z}/\text{H}] = -0.2 \dots -0.3$. In the inner part of the disk ($r = 7''$ – $16''$), the stellar population is old, the abundance ratio reaches $[\text{Mg}/\text{Fe}] = +0.2$, and the metallicity decreases to $[\text{Z}/\text{H}] < -0.33$, demonstrating the properties that exactly match the stellar population characteristics of the globular clusters in the bulge of our Galaxy, which are also plotted in our age-diagnostic diagrams for comparison. Such characteristics imply a brief single starburst that took place more than 10 Gyr ago and formed the large-scale stellar disk of NGC 4324. In the ring-dominated area of the disk ($r = 17''$ – $35''$), the dominant stellar population is also old, though slightly younger than in the inner disk, and the mean chemical properties of the stars are nearly the same.

NGC 7808. In NGC 7808, we have succeeded in distinguishing the nucleus(+bulge), disk, and inner star-forming ring (the outer UV-bright ring at $r > 23''$ (Ilyina & Sil'chenko 2011) is too faint in continuum, and we cannot derive its stellar population properties). In this galaxy, we had two long-slit cross sections in two different slit orientations, but because the velocity profiles appear to be identical, we added both spectra before analyzing the stellar population properties. As a result, the stellar population characteristics are taken under some 36° to the major axis. In Figure 9, one can see that in the center ($r < 2''$), the mean age of the stellar population is 4–5 Gyr, the abundance ratio $[\text{Mg}/\text{Fe}] \approx +0.1$, and the stellar metallicity is close to the solar one. All of these characteristics point at prolonged star formation that stopped there about 2.5 Gyr ago. The history of the nucleus in NGC 7808 resembles that of the nucleus of NGC 809. In the inner disk, at $r = 5''$ – $9''5$, the mean age of the stellar population is 8 Gyr, the abundance ratio increases to $[\text{Mg}/\text{Fe}] \geq +0.3$, and the metallicity decreases to $[\text{Z}/\text{H}] \leq -0.33$. And, at the radii $10'' \leq r < 15''$, we observe a

ringlike region, this time with star formation, where the mean age of the stellar population drops to 3 Gyr, but the abundances are the same as in the inner stellar disk. Presumably, the ringlike star formation burst is brief and has happened at least twice at the same radius, about 2.5 Gyr ago and quite recently (since we observe the $H\alpha$ emission line excited by young stars in the ring). As for NGC 2697, we conclude that the disk formation in NGC 7808 has evolved as inside-out.

PGC 48114. In PGC 48114, we inspect the nucleus and two stellar rings—a red one at $r = 3''\text{--}10''$ (1.5–4.8 kpc) and one at $r = 11''\text{--}17''$, the latter also corresponding to the UV-bright area. The double ring in PGC 48114 may be classified as R_1R_2 ; this time, a weak bar presence can be suspected. In the outer bright inhomogeneous ring, starting from $r > 12''$, the strong emission lines have been detected as partially excited by the star-forming process (along our slit—only to the west of the nucleus). In the center ($r < 2''$) of PGC 48114, the mean age of the stellar population is about 5 Gyr, the abundance ratio $[\text{Mg}/\text{Fe}] \approx +0.1$, and the metallicity $[Z/\text{H}] = +0.3$ —typical values for the nuclei of lenticular galaxies (Sil'chenko 2006, 2016). However, the low $[\text{Mg}/\text{Fe}]$, within the range of $0 \dots +0.1$, kept all along the galaxy is quite untypical for the contemporary lenticular galaxies (Sil'chenko et al. 2012); it implies an extended star formation epoch in the disk. The inner elliptical ring is rather old, $T = 9 \pm 5$ Gyr, with the typical low stellar metallicity, $[Z/\text{H}] = -0.3$. However, in the area of the outer, star-forming ring, the mean stellar age drops to 3 Gyr, and the metallicity drops also, to $[Z/\text{H}] < -1$.

ORCID iDs

Alexei Yu. Kniazev  <https://orcid.org/0000-0001-8646-0419>
Olga K. Sil'chenko  <https://orcid.org/0000-0003-4946-794X>

References

Ahn, C. P., Alexandroff, R., Allende Prieto, C., et al. 2012, *ApJS*, 203, 21
Alatalo, K., Davis, T. A., Bureau, M., et al. 2013, *MNRAS*, 432, 1796
Allen, M. G., Groves, B. A., Dopita, M. A., et al. 2008, *ApJS*, 178, 20
Athanasoula, E., Bosma, A., Creze, M., et al. 1982, *A&A*, 107, 101
Bai, Y., Zou, H., Liu, J., et al. 2015, *ApJS*, 220, 6
Baldwin, J. A., Phillips, M. M., & Terlevich, R. 1981, *PASP*, 93, 5
Beasley, M. A., Brodie, J. P., Strader, J., et al. 2004, *AJ*, 128, 1623
Bertola, F., Buson, L. M., & Zeilinger, W. W. 1992, *ApJL*, 401, L79
Bigiel, F., Leroy, A. K., Walter, F., et al. 2011, *ApJL*, 730, L13
Binette, L., Magris, C. G., Stasińska, G., et al. 1994, *A&A*, 292, 13
Bothwell, M. S., Kennicutt, R. C., & Lee, J. C. 2009, *MNRAS*, 400, 154
Brown, T. M., Baliber, N., Bianco, F. B., et al. 2013, *PASP*, 125, 1031
Buckley, D. A. H., Swart, G. P., & Meiring, J. G. 2006, *Proc. SPIE*, 6267, 62670Z
Burgh, E. B., Nordsieck, K. H., Kobulnicky, H. A., et al. 2003, *Proc. SPIE*, 4841, 1463
Buta, R., & Combes, F. 1996, *FCPh*, 17, 95
Buta, R., Laurikainen, E., Salo, H., et al. 2010, *ApJ*, 721, 259
Buta, R. J. 2017, *MNRAS*, 471, 4027
Chiappini, C., Matteucci, F., & Gratton, R. 1997, *ApJ*, 477, 765

Comerón, S., Salo, H., Laurikainen, E., et al. 2014, *A&A*, 562, A121
Cortese, L., & Hughes, T. M. 2009, *MNRAS*, 400, 1225
Crawford, S. M., Still, M., Schellart, P., et al. 2010, *Proc. SPIE*, 7737, 773725
Davé, R., Finlator, K., & Oppenheimer, B. D. 2012, *MNRAS*, 421, 98
Davis, T. A., Alatalo, K., Sarzi, M., et al. 2011, *MNRAS*, 417, 882
de Vaucouleurs, G., de Vaucouleurs, A., Corwin, H. G., Jr., et al. 1991, Third Reference Catalogue of Bright Galaxies, Vol. I, II, III (New York: Springer)
Faber, S. M., Friel, E. D., Burstein, D., et al. 1985, *ApJS*, 57, 711
Fall, S. M., & Efstathiou, G. 1980, *MNRAS*, 193, 189
Fraternali, F., & Binney, J. J. 2006, *MNRAS*, 366, 449
Gil de Paz, A., Boissier, S., Madore, B. F., et al. 2007, *ApJS*, 173, 185
Houck, J. C., & Bregman, J. N. 1990, *ApJ*, 352, 506
Ilyina, M. A., & Sil'chenko, O. K. 2011, *AstL*, 37, 589
Ilyina, M. A., Sil'chenko, O. K., & Afanasiev, V. L. 2014, *MNRAS*, 439, 334
Katkov, I. Y., Kniazev, A. Y., & Sil'chenko, O. K. 2015, *AJ*, 150, 24
Katkov, I. Y., Sil'chenko, O. K., & Afanasiev, V. L. 2014, *MNRAS*, 438, 2798
Kauffmann, G., Heckman, T. M., Tremonti, C., et al. 2003, *MNRAS*, 346, 1055
Kennicutt, R. C., & Evans, N. J. 2012, *ARA&A*, 50, 531
Kewley, L. J., Dopita, M. A., Sutherland, R. S., et al. 2001, *ApJ*, 556, 121
Kewley, L. J., Groves, B., Kauffmann, G., et al. 2006, *MNRAS*, 372, 961
Kniazev, A. Y., Zijlstra, A. A., Grebel, E. K., et al. 2008, *MNRAS*, 388, 1667
Kobulnicky, H. A., Nordsieck, K. H., Burgh, E. B., et al. 2003, *Proc. SPIE*, 4841, 1634
Kostiuk, I. P., & Sil'chenko, O. K. 2015, *AstBu*, 70, 280
Kostyuk, I. P. 1975, *SoSAO*, 13, 45
Kudritzki, R.-P., Ho, I.-T., Schruha, A., et al. 2015, *MNRAS*, 450, 342
Kuijken, K., Fisher, D., & Merrifield, M. R. 1996, *MNRAS*, 283, 543
Laurikainen, E., Salo, H., Athanassoula, E., et al. 2013, *MNRAS*, 430, 3489
Lee, J. C., Gil de Paz, A., Kennicutt, R. C., Jr., et al. 2011, *ApJS*, 192, 6
Lilly, S. J., Carollo, C. M., Pipino, A., et al. 2013, *ApJ*, 772, 119
Marinacci, F., Binney, J., Fraternali, F., et al. 2010, *MNRAS*, 404, 1464
Marino, A., Bianchi, L., Rampazzo, R., et al. 2011, *ApJ*, 736, 154
Marino, R. A., Rosales-Ortega, F. F., Sánchez, S. F., et al. 2013, *A&A*, 559, A114
Matteucci, F., & Greggio, L. 1986, *A&A*, 154, 279
Morrissey, P., Conrow, T., Barlow, T. A., et al. 2007, *ApJS*, 173, 682
Nair, P. B., & Abraham, R. G. 2010, *ApJS*, 186, 427
O'Donoghue, D., Buckley, D. A. H., Balona, L. A., et al. 2006, *MNRAS*, 372, 151
Osterbrock, D. E., & Ferland, G. J. 2006, *Astrophysics of Gaseous Nebulae and Active Galactic Nuclei* (2nd ed.; Sausalito, CA: Univ. Science Books)
Pettini, M., & Pagel, B. E. J. 2004, *MNRAS*, 348, L59
Pogge, R. W., & Eskridge, P. B. 1987, *AJ*, 93, 291
Pogge, R. W., & Eskridge, P. B. 1993, *AJ*, 106, 1405
Pogge, R. W., & Eskridge, P. B. 1999, in *ASP Conf. Ser. 163, Star Formation in Early Type Galaxies*, ed. P. Carral & J. Cepa (San Francisco, CA: ASP), 174
Sage, L. J., & Welch, G. A. 2006, *ApJ*, 644, 850
Salim, S., Fang, J. J., Rich, R. M., et al. 2012, *ApJ*, 755, 105
Schommer, R. A., & Sullivan, W. T., III 1976, *ApL*, 17, 191
Sheth, K., Regan, M., Hinz, J. L., et al. 2010, *PASP*, 122, 1397
Sil'chenko, O., Kostiuk, I., Burenkov, A., et al. 2018, *A&A*, 620, L7
Sil'chenko, O. K. 2006, *ApJ*, 641, 229
Sil'chenko, O. K. 2016, *AJ*, 152, 73
Sil'chenko, O. K., Proshina, I. S., Shulga, A. P., et al. 2012, *MNRAS*, 427, 790
Smith, R. J., Lucey, J. R., Hudson, M. J., et al. 2009, *MNRAS*, 392, 1265
Stasińska, G., & Sodr , L., Jr. 2001, *A&A*, 374, 919
Thomas, D., Maraston, C., & Bender, R. 2003, *MNRAS*, 339, 897
Welch, G. A., & Sage, L. J. 2003, *ApJ*, 584, 260
Worthey, G., Faber, S. M., Gonzalez, J. J., et al. 1994, *ApJS*, 94, 687
Worthey, G., & Ottaviani, D. L. 1997, *ApJS*, 111, 377